Hexatic order in thin smectic-*F* liquid-crystal films

Q. J. Harris, D. Y. Noh,* D. A. Turnbull,† and R. J. Birgeneau
Department of Physics, Massachusetts Institute of Technology, Cambridge, Massachusetts 02139
(Received 3 February 1995)

We report a synchrotron x-ray study of the stacked hexatic smectic-*F* phase and the smectic-*F* (Sm-*F*)→smectic-*C* (Sm-*C*) phase transition in ~200 and ~60 molecular layer thick films of terephthal-bis-(20)-alkylanilines. A diffraction geometry is developed to facilitate the measurements on freely suspended liquid-crystal films. Deep in the hexatic Sm-*F* phase, both films show a high degree of orientational order. The effects of the surface ordering field in thin liquid-crystal films are discussed. In both samples, the phase transition from the Sm-*F* phase to the Sm-*C* phase is strongly first order, in contrast with the continuous Kosterlitz-Thouless hexatic-isotropic phase transition predicted for two-dimensional systems.

PACS number(s): 64.70.Md, 61.30.Gd

I. INTRODUCTION

Hexatic phases of liquid crystals are characterized by liquidlike short-range positional order and solidlike long-range bond orientational order in three dimensions or quasi-long-range bond orientational order in two dimensions. Although the positions of the constituent particles are not well defined in the hexatic phase, there is well-defined order in the direction of the local crystalline axes. Ever since the invention of the concept of defect-mediated melting in two dimensions which predicts the existence of an intermediate hexatic phase [1–4], substrate-free liquid-crystal films have been used as model systems [5] to investigate the nature of hexatic phases and their transitions to the bounding solid and isotropic liquid phases.

Thermotropic liquid crystals are typically made up of long rodlike organic molecules that form various phases. In the smectic phases, the molecules segregate into layers, lining up parallel to each other. The smectic-*C* phase (Sm-*C*) may be described heuristically as stacked liquid smectic layers with a nonzero tilt angle between the long axis of the molecules and the layer normal. The smectic-*F* phase (Sm-*F*) is a more ordered phase than the Sm-*C* phase. It is a three-dimensional hexatic phase with long-range bond orientational order but short-range positional order [6]. The Sm-*F* phase freezes into the true crystalline smectic-*G* (Sm-*G*) phase at lower temperatures. High quality single domain samples are indispensable in studying hexatic phases since the mosaic structure of a multi-domain sample will broaden the characteristic hexatic orientational order. Brock *et al.* [7,8] introduced a technique for making single domain samples which involved freely suspended liquid-crystal films cooled from the untilted smectic-*A* (Sm-*A*) phase to the tilted Sm-*C* phase in the presence of a magnetic field. This technique also allows one to make samples with various thickness, which is essential to this study.

The phase behavior of hexatic and solid phases in two dimensions is quite different from that in three dimensions. In two dimensions, the increased thermal fluctuations destroy conventional long-range order in the hexatic phase causing the correlations of the hexatic order to decay to zero algebraically with increasing distance. This algebraic decay state is sometimes called quasi-long-range order. The difference between hexatic order in two and three dimensions has been demonstrated experimentally by x-ray diffraction [8,9] and electron diffraction [10]. The divergent thermal fluctuations in two dimensions may also alter the nature of the hexatic-liquid transition. Experimentally, the hexatic-liquid transition is found to be continuous, but has a tricritical specific-heat component $\alpha \simeq 0.5$ [11], or weakly first order in three-dimensional systems, whereas in two dimensions it may show continuous Kosterlitz-Thouless behavior [1].

It is clearly an intriguing problem to study the evolution of the hexatic phases and phase transitions as the dimensionality of a system changes from three (bulk samples) to two dimensions (thin films). Interesting results on dimensional crossover in the crystalline order in solid films have already been obtained by Noh *et al.* [12]. There is, however, an extra complication in the phase behavior of thin film liquid-crystal materials. Specifically, two peaks rather than one are observed in heat capacity measurements of the isotropic-hexatic transition in freely suspended films [13,14]; this indicates that the surface of the film develops bond orientational order prior to the bulk. Surface ordering is a common feature in freely suspended liquid-crystal films, due to the surface tension that constrains fluctuations near the surface. As the thickness of the system decreases, the surface layers play a more and more significant role, thus complicating the phase behavior of the intermediate thickness system. Understanding the competition between the dimensionality and the surface ordering field is one motivation of this

*Present address: Exxon Research and Engineering Co., Clinton Township, Rte. 22 East, Annandale, NJ 08801.
†Present address: Department of Physics, University of Illinois at Urbana-Champaign, Urbana, IL 61801.

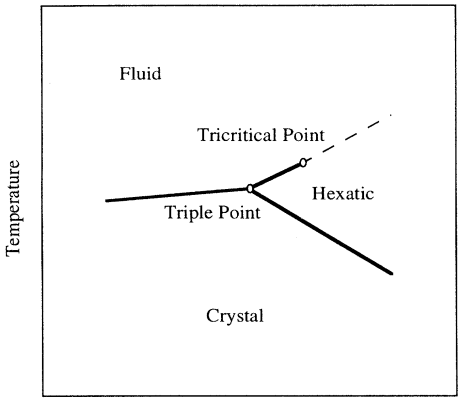

FIG. 1. Generic phase diagram near the fluid-hexatic-crystal coexistence triple point. The broken (full) lines indicate second (first) order transitions [16]. When the rounding effect of the tilted field is ignored, and this is also the generic phase diagram near the Sm-*C*-Sm-*F*-Sm-*G* triple point.

study.

In this paper, we present an x-ray diffraction study of the hexatic (Sm-*F*) → liquid (Sm-*C*) transition in films of terephthal-bis-(20)-alkylanilines (TB5A) which are 60 molecular layers thick and 200 molecular layers thick. Noh *et al.* [15] studied the phase diagram, Fig. 1, of the three-dimensional limit of the TB*n*A system near a triple point where the solid, hexatic, and liquid phases meet. They found that the transition between the liquid Sm-*C* phase and the hexatic Sm-*F* phase is first order in TB5A, which is close to the triple point, but possibly second order in both TB6A and TB7A, which are away from the triple point. This result is consistent with the prediction by Aharony *et al.* [16] of a tricritical point near a triple point in the temperature and concentration phase diagram. Aharony *et al.* [16] argue that the transition becomes first order due to the coupling between fluctuations in the crystalline order and the hexatic order as one approaches the triple point. Hence, another motivation of this study is to understand the hexatic phase behavior as we decrease the sample thickness to the two-dimensional limit.

This paper is organized as follows. In Sec. II, we present a description of the experimental details including our development of a new diffraction geometry to facilitate measurements on hexatic films. The experimental results and the data analysis are discussed in Sec. III. We summarize this paper in Sec. IV.

II. EXPERIMENTAL DETAILS

This experiment was carried out on the MIT/IBM beamline X20B at the National Synchrotron Light Source (NSLS) at Brookhaven National Laboratory. The white x-ray beam from a bending magnet was horizontally focused and monochromatized by a singly bent Si(111) crystal. Further energy of the incident x-ray photons was fixed at 17.4 keV. Further details regarding X20B can be found in Ref. [17]. A set of slits, 1×1 mm^2, directly in front of the sample chamber determined the illuminated area. We carefully evacuated all flight paths and shielded off as much air scattering as possible. The diffraction intensity was recorded by a detector manufactured by Bicron. Since no analyzer was used in the experiment, the momentum space resolution function was primarily determined by a set of slits right in front of the detector, which was 2×2 mm^2.

The samples were prepared by using the freely suspended film technique in a two-stage oven [9]. TB5A films were drawn in the Sm-*A* phase at about 180 °C and annealed until uniform in thickness, which was determined by visual inspection. Two $SmCo_5$ magnets were utilized to produce roughly 1000 G magnetic field at the sample. The field served to align the molecular tilt direction in the cooling from the Sm-*A* to the Sm-*C* phase. The alignment of the molecular tilt direction in turn provided an ordering field to lock the direction of the orientational order [18]. The sample chamber was initially evacuated and then filled with N_2 gas at 1 Torr to minimize any sample degradation by ambient water vapor and to reduce the residual air scattering. The sample temperature was controlled to within ±50 mK. A detailed description of the sample chamber and the sample preparation technique can be found in Ref. [19]. The chamber was mounted such that the x-ray diffraction occurred in transmission through the film.

The thickness of the samples was determined by various methods. For the 60-layer film, the Bragg peak in the solid Sm-*G* phase showed broadening due to the finite thickness of the sample. We determined the thickness of that film from the width of the Bragg peak in the solid Sm-*G* phase. One may also use the color of the light reflection from the sample to estimate the thickness of the sample. The color of the 60-layer film was purple, consistent with the color diagram by Sorensen *et al.* [20] for ~60-layer films. For the 200-layer film, however, it was difficult to apply either of the above-mentioned methods to determine the thickness. The finite-size broadening was so small that it was difficult to separate it from instrumental resolution effects. Thus, in the end, we determined the thickness of this film by scaling the x-ray diffraction intensity in the fluid Sm-*A* phase to that of the 60-layer-thick film. In the isotropic fluid phase the positions of the molecules have no correlation and the diffraction intensity is simply proportional to the number of scatterers, which in turn is proportional to the thickness of the sample, provided that the illuminated area is kept fixed.

As stated above, the Sm-*C* phase can be naively described as a stack of two-dimensional fluid layers where the molecules are tilted with respect to the layer normal. The diffraction pattern of the Sm-*C* phase is, therefore, a tilted fluid ring—a two-dimensional nearly isotropic cylinder modified by the form factor of the tilted molecules [21]. It is important to note that the *ring* is what actually tilts. It is not the intersection of a cylinder with a tilted plane, rather it is a *tilted circle.* This counterintuitive effect is due to the close packing of the molecules. The nearest neighbor distance, measured perpendicular to the long molecular axis, is a constant in the phase transition from the untilted Sm-*A* phase to the tilted Sm-*C*

phase [21]. In the hexatic Sm-*F* phase, the tilted ring condenses into six diffuse spots as the bond orientational order develops, breaking the rotational symmetry. Technically, there should also be induced orientational order in the Sm-*C* phase due to the coupling between the molecular tilt and the hexatic order parameter [18]. This is indeed the case with racemic 4-(2′-methylbutyl)phenyl 4′-(octyloxy)-(1,1′)-biphenyl-4-carboxylate (8OSI), in which significant bond orientational order persists well into the Sm-*C* phase [7,8]. However, this induced order was too weak to observe in this study. The bond orientational order may be characterized quantitatively by analyzing the profiles of these spots.

To study the diffraction profile of the diffuse spots, conventionally angular scans are performed by rotating the sample in such a way as to measure the diffraction intensity as a function of the momentum transfer **q** along the tilted ring. This is referred to in the literature [7–9,12] as a χ scan because the scan is carried out by rotating the sample along the χ circle of a Huber four-circle goniometer, with some θ_s motion to account for the fact that the ring (in the Sm-*C* phase) or the diffuse spot (in the Sm-*F* phase) is tilted in reciprocal space. While this method is technically easy and straightforward, it always introduces the possibility of an artificial broadening generated by the liquid sample motion. This artificial broadening is especially serious for systems where the coupling between the molecular tilt and crystalline axes directions is weak as in the TB*n*A materials.

In order to minimize any artificial disruption of the orientational order due to the sample motion, we introduced the following experimental geometry. Instead of rotating the sample along the χ circle through angles as large as 60° in the course of a scan, the detector itself was rotated together with a very limited θ motion of the sample such that the momentum transfer to the sample **q** could be scanned around the tilted ring. The θ motion was about an axis in the plane of the sample and therefore did not disrupt the intraplanar orientational order. Figure 2(a) illustrates the experimental configuration. The outgoing flight path and the detector were mounted on a special apparatus, as shown in Fig. 2(b), rather than the detector arm of a conventional four-circle Huber goniometer. This allowed the detector to move along the circumference of the circle, while the flight path and the detector always pointed directly to the sample position. We label this new diffraction geometry an "*x* scan." Figure 2(b) shows the end view of the apparatus for an "*x* scan." In the experiment, the rotational axis of the arc *MN*, that is, perpendicular to the paper, was aligned collinear with the incident x-ray beam. To start with, we aligned the flight path and the detector on the detector arm, which is also called the 2θ arm, of a Huber goniometer to locate the correct 2θ angle, as determined by the momentum transfer, $q = 2k \sin(2\theta/2)$; the holder of the apparatus for the "*x* scan" was aligned parallel to the detector arm. We then transferred the flight path and the detector from the Huber 2θ arm onto the apparatus and moved the Huber detector arm away. Theoretically, the detector rotation device could have been mounted directly on the 2θ arm of the Huber goniometer. This alternative scheme was necessitated by the weight and geometry of the particular rotation device available to us at the time of the experiment. As illustrated in Fig. 2(b), while *R* moves along the arc *MN*, the detector itself makes a circular motion around the rotation center *O*, as shown in Fig. 2(a). The 2θ angle, that is, the angle between the outgoing diffraction beam and the incident x-ray beam, thus remains fixed in the course of a scan.

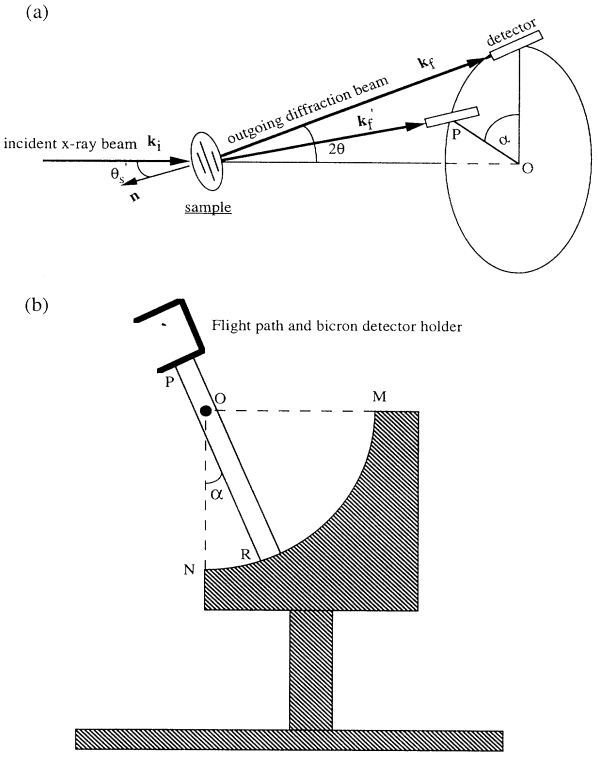

FIG. 2. (a) The experimental layout of the new geometry—"*x* scan." When one rotates the detector along the circumference of the circle, one changes the outgoing diffraction beam direction along the cone, that is, the detector itself makes a circular motion around the rotation center *O*. The 2θ angle, which is the angle between the outgoing diffraction beam and the incident x-ray beam, remains fixed in the course of a scan. (b) An end view of the apparatus used in the experiment to carry out an "*x* scan." When *R* moves along the arc *MN*, the detector makes a circular motion around the center *O*.

In order to understand how this geometry achieves the same goal as a conventional χ scan, let us first briefly outline how a χ-scan probes the bond orientational order. In Fig. 3(a), **x**, **y**, and **z** are the coordinates in the laboratory frame, while **H**, **K**, and **L** are the coordinates in the reciprocal space fixed on the sample frame. The momentum transfer in a χ-scan $\mathbf{q}_\chi = \mathbf{k}_f - \mathbf{k}_i$ is given by

$$\mathbf{q}_\chi = -2k \sin^2\left(\frac{2\theta}{2}\right)\hat{\mathbf{x}} + 2k \sin\left(\frac{2\theta}{2}\right)\cos\left(\frac{2\theta}{2}\right)\hat{\mathbf{y}}$$
$$= q\cos\omega\sin(\chi)\hat{\mathbf{H}} + q\cos\omega\cos\chi\hat{\mathbf{K}} + q\sin(\omega)\hat{\mathbf{L}}\ , \qquad (1)$$

where $q \equiv 2k \sin(2\theta/2)$, $\omega \equiv \theta_s - (2\theta/2)$, and θ_s is the an-

gle between the incident x-ray beam and the film surface normal, 2θ is the detector angle.

In the "x-scan" geometry, one rotates the detector instead of the sample, so the final momentum $\mathbf{k}_f$ is no longer fixed in the laboratory frame, but the 2θ angle, that is the angle between the outgoing diffraction beam and the incident x-ray beam, remains fixed. Therefore, the magnitude of the moment transfer to the sample is kept constant. This is in contrast with the situation discussed above where the detector is held fixed and only the sample is rotated. In that case, the final momentum is fixed in the laboratory frame so that, in effect, the reciprocal space rotates in the laboratory frame [Fig. 3(a)].

When we rotate the detector along the circumference through an angle α, as in Figs. 2(a) and 2(b), the momentum of the outgoing diffraction beam becomes $\mathbf{k}'_f$ instead of $\mathbf{k}_f$, as shown in Fig. 3(b). We therefore have for the momentum transfer in an "x-scan" $\mathbf{q}_{\text{new}}=\mathbf{k}'_f-\mathbf{k}_i$:

$$\mathbf{q}_{\text{new}}=-2k\sin^2\left[\frac{2\theta}{2}\right]\hat{\mathbf{x}}+2k\sin\frac{2\theta}{2}\cos\frac{2\theta}{2}\cos(\alpha)\hat{\mathbf{y}}+2k\sin\frac{2\theta}{2}\cos\frac{2\theta}{2}\sin(\alpha)\hat{\mathbf{z}}$$

$$=-q\cos\frac{2\theta}{2}\sin(\alpha)\hat{\mathbf{H}}+q\left[\sin\frac{2\theta}{2}\sin\theta'_s+\cos\frac{2\theta}{2}\cos\theta'_s\cos\alpha\right]\hat{\mathbf{K}}+q\left[\cos\frac{2\theta}{2}\sin\theta'_s\cos\alpha-\sin\frac{2\theta}{2}\cos\theta'_s\right]\hat{\mathbf{L}}\,, \qquad (2)$$

where $q\equiv 2k\sin(2\theta/2)$ and α is the angle between $\mathbf{k}_f$ and $\mathbf{k}'_f$.

Comparing Eq. (1) and Eq. (2), we can easily see that there is a one-to-one correspondence between $(2\theta,\theta_s,\chi)$ and $(2\theta,\theta'_s,\alpha)$. Hence, this demonstrates how one can rotate the detector instead of the sample to arrive at the same position (h,k,l) in reciprocal space, that is, to achieve the same momentum transfer $\mathbf{q}$.

III. RESULTS AND DATA ANALYSIS

We first discuss the development of the hexatic order across the Sm-$C\rightarrow$Sm-F transition. Figure 4 shows a series of angular scans along the tilted ring obtained using the "x-scan" technique at several temperatures across the transition. In presenting the results, although the scans were carried out by rotating the detector in the fashion described above, the data have been converted from the diffraction intensity as a function of $(2\theta,\theta'_s,\alpha)$ to the diffraction intensity as a function of $(2\theta,\theta_s,\chi)$ according to Eqs. (1) and (2). At high temperatures, the angular scans were flat, independent of direction, corresponding to an isotropic fluid diffraction pattern. A longitudinal scan, that is, a diffraction profile across the ring, illustrated in Fig. 5(a), showed a broad peak characteristic of a fluid phase. The positional correlation length obtained from a fit to a Lorentzian was $\sim$20 Å. As the temperature was lowered, definite peaks appeared every 60° in angular scans, indicating the development of long-range orientational order. The longitudinal scan, as shown in Fig. 5(b), became significantly sharper at low temperatures, although it was still much wider than the instrumental resolution; this implies that the positional correlation length grows but is still short range. The positional correlation length deep in the Sm-F phase was about 150 Å. In previous studies, it had been found that the positional correlation length increased up to $\sim$100 Å in the hexatic phase of thermotropic liquid crystals [22]. Comparing with the data of Noh *et al.* on thick TB5A films [15], one can conclude that in these TB5A thin

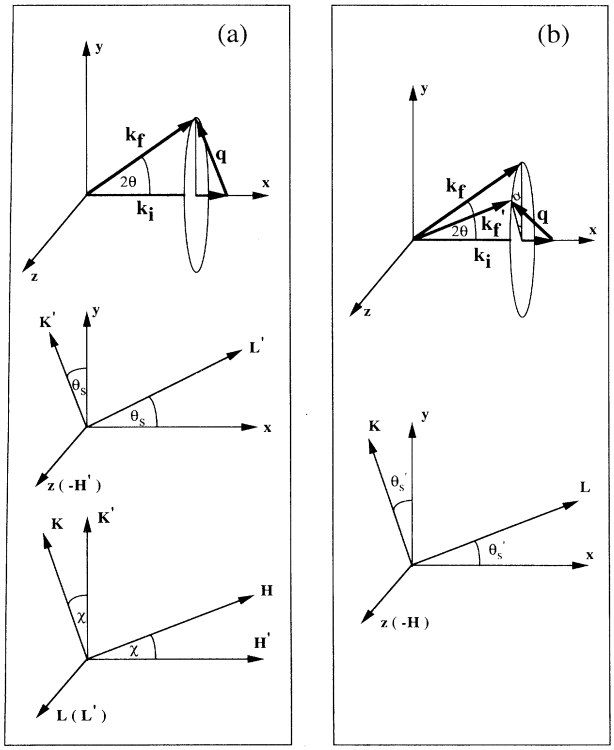

FIG. 3. (a) The relations among the coordinates in a χ scan. $\mathbf{q}=\mathbf{k}_f-\mathbf{k}_i$ in the first plot. In a χ scan, the detector is fixed in the laboratory frame; it is the reciprocal space that rotates in the laboratory frame. From the second and third plot on the left panel one has $\hat{\mathbf{x}}=-\sin\theta_s\sin(\chi)\hat{\mathbf{H}}-\sin\theta_s\cos\chi\hat{\mathbf{K}}+\cos\theta_s\hat{\mathbf{L}}$; $\hat{\mathbf{y}}=\cos\theta_s\sin(\chi)\hat{\mathbf{H}}+\cos\theta_s\cos(\chi)\hat{\mathbf{K}}+\sin(\theta_s)\hat{\mathbf{L}}$; $\hat{\mathbf{z}}=-\cos(\chi)\hat{\mathbf{H}}+\sin(\chi)\hat{\mathbf{K}}$. (b) the relations among the coordinates in an "x scan." In an x scan, the detector itself rotates in the laboratory frame, when it moves along the circumference through an angle α, $\mathbf{q}=\mathbf{k}'_f-\mathbf{k}_i$ as shown in the first plot on the right panel. The second plot on the right panel gives the relation between the reciprocal space and the coordinates fixed in the laboratory frame: $\hat{\mathbf{x}}=\cos(\theta'_s)\hat{\mathbf{L}}-\sin(\theta'_s)\hat{\mathbf{K}}$; $\hat{\mathbf{y}}=\sin(\theta'_s)\hat{\mathbf{L}}+\cos(\theta'_s)\hat{\mathbf{K}}$; $\hat{\mathbf{z}}=-\hat{\mathbf{H}}$.

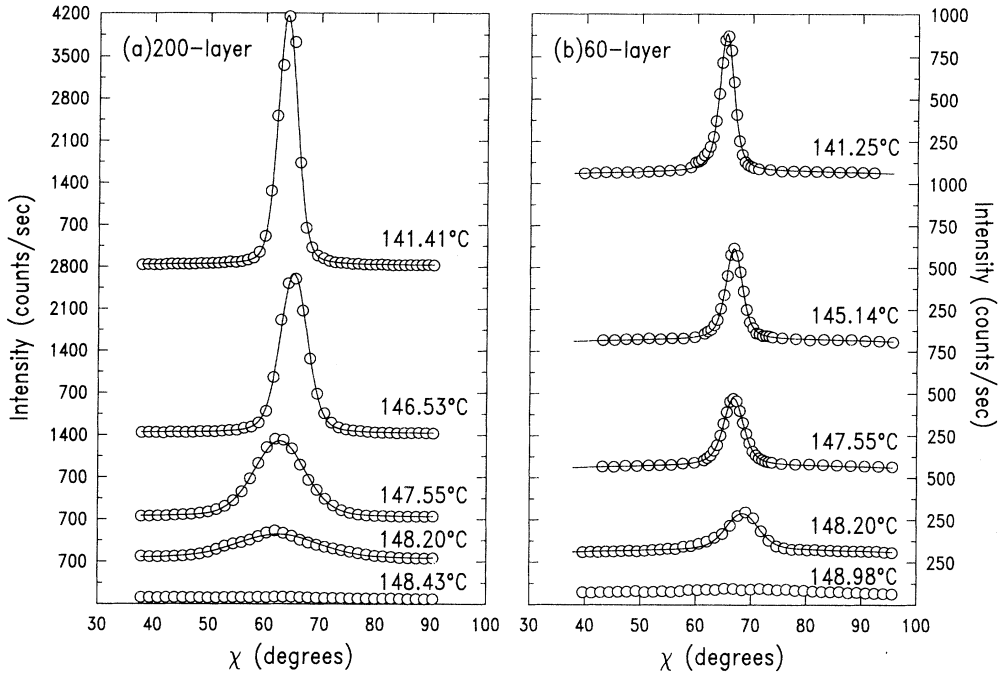

FIG. 4. Angular scans obtained using the technique "x scan" across the Sm-$F \rightarrow$Sm-C phase transition. The data have been converted from the diffraction intensity as a function of $(2\theta, \theta_s', \alpha)$ to the diffraction intensity as a function of $(2\theta, \theta_s, \chi)$. In both samples, there are definite peaks in angular scans deep in the Sm-F phase and as the samples undergo the Sm-$F \rightarrow$Sm-C phase transition, the peaks disappear abruptly. There is no measurable bond orientational order in the Sm-C phase, in contrast with the experimental results on 8OSI [7,8]. The solid line is the best fit to Eq. (3). [We also fitted the data to Eq. (3), assuming the harmonics are related according to Eq. (4); the fits yield identical lines.] (a) ~200-layer film. (b) ~60-layer film.

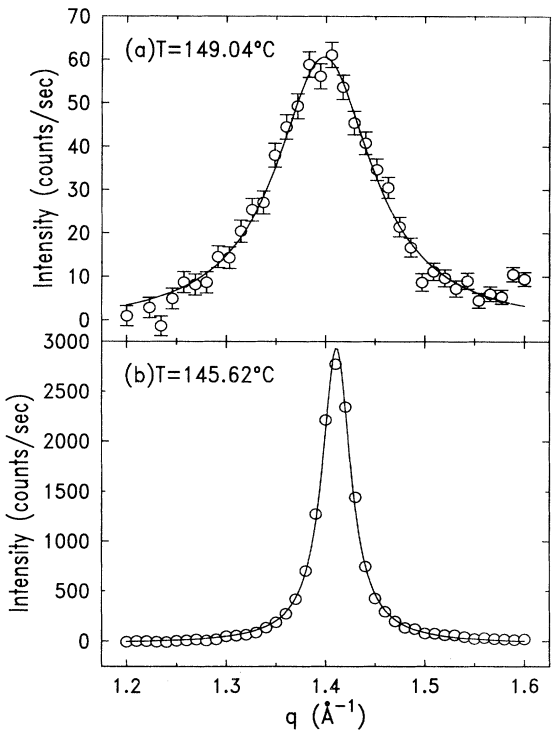

FIG. 5. Representative longitudinal scans of the ~200-layer film. (a) Representative longitudinal scan in the liquid Sm-C phase. The solid line is the best fit of a Lorentzian to the data. (b) Representative longitudinal scan in the hexatic Sm-F phase. The solid line is the best fit of a Lorentzian. In both plots, the background is subtracted.

films, the phase behavior is identical to that in bulk samples. This agrees with the data of Brock *et al.* on 8OSI [8], in which the same set of phases was observed in films of various thickness. However, very different phase behavior as a function of thickness was observed in liquid-crystal 4-n-heptyloxybenzylidene-4-n-heptylaniline (7O.7) by Sirota *et al.* [23]. In this case, hexatic Sm-F and Sm-I phases were observed only in films thinner than ~280 and ~25 layers, respectively, while thick films did not display any hexatic order.

The Sm-$C \rightarrow$Sm-F transition was abrupt in both the 60- and 200-layer films. To follow the development of the hexatic order quantitatively, we have fit the data to a Fourier cosine series,

$$S(\chi) = I_0 \left[\frac{1}{2} + \sum_{n=1}^{\infty} C_{6n} \cos 6n(\chi - 60°) \right] \times (\cos\theta_s)^{-1} + I_{\text{bg}} \, . \tag{3}$$

Here the factor $(\cos\theta_s)^{-1}$ is the illuminated volume correction [8] and I_{bg} is the experimentally measured background. All of the C_{6n} are normalized such that $0 \le C_{6n} \le 1$. When all of the $C_{6n} = 1$, Eq. (3) is a periodic δ function, that is, the bond orientational order is perfect. When all of the $C_{6n} = 0$, the diffraction profile is uniform in angle χ after taking the background into account, that is, there is no bond orientational order. Each of the $\{C_{6n}\}$ represents an independent order parameter associated with the amount of the $6n$-fold order in the sample [8,9]. The temperature dependences of the first several $\{C_{6n}\}$ are shown in Fig. 6. It is obvious that the transition is strongly first order in both the 200- and 60-laver

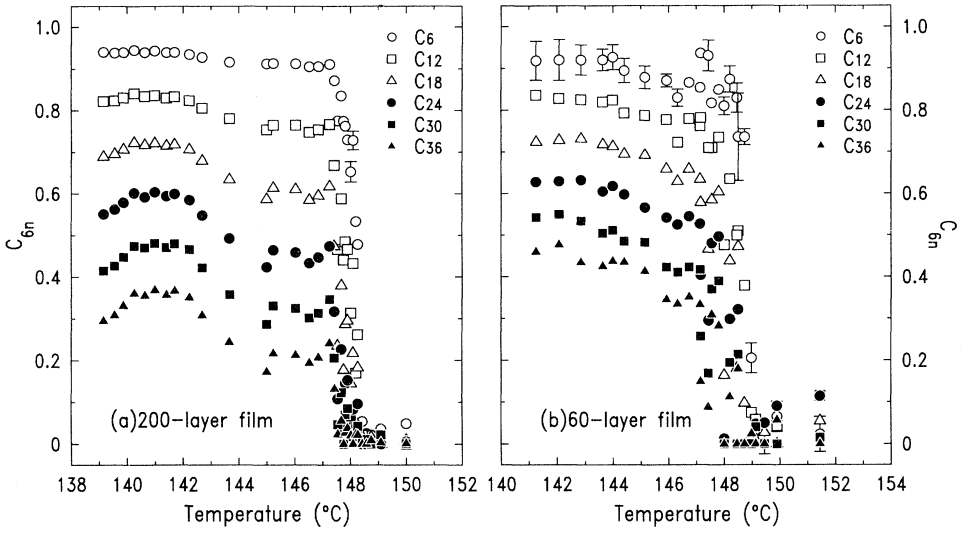

FIG. 6. Temperature dependence of the first six order parameters in both samples. All the order parameters drop to zero abruptly at T_C. The transition is strongly first order. (a) ~200-layer film. (b) ~60-layer film.

films. There are discontinuous jumps not only in the primary order parameter C_6, but also in all of the higher harmonic order parameters C_{6n}. High order harmonics always provide a more rigorous test for the first order character of a transition compared with the primary order parameter since they are more susceptible to the fluctuations. Equivalently, the order parameter exponents β_n are much larger than β_1. The presence of significant higher order harmonics in both the 200- and 60-layer-thick TB5A films is in contrast with the results of Brock *et al.* on 23-layer-thick film of 8OSI [8], in which all the C_{6n} terms except those for $n=1,2$ were found absent. We would like to note here that generally the broader the angular scan, the fewer the C_{6n} present. As we shall discuss later, we have observed much sharper angular scans in this study than the results on 8OSI by Brock *et al.* [8] for both thick and thin films.

We also observed some evidence for floating hexatic islands coexisting with the isotropic fluid phase in the films very close to the transition temperature. The intensities and the peak positions appeared to fluctuate randomly. Subsequent scans at a fixed temperature showed different profiles. This is a unique feature of a first order transition and the concomitant two phase coexistence in liquid-crystal films. The scans shown in Fig. 4 are averages of ten repeated scans at each temperature.

The value of C_6 deep in the Sm-F phase was close to 1, indicating that the hexatic order was very well established in both samples. Well-defined hexatic order was also evinced by the large values of C_{6n} for the higher harmonics as well. The HWHM (half width at half maximum) of the angular scans of the 200-layer-thick film in Sm-F was only 2.3° at low temperatures. The 60-layer-thick film had an even smaller HWHM of 1.9°. It is important to observe that the angular scans of these films show much sharper peaks than those of angular scans of any other substrate-free hexatic phases, including 8OSI films [8,9] and the thick bulk samples of TB5A [15]. This is surprising since in thin films, we expect that the larger amplitude thermal fluctuations compared with those in the bulk would decrease the orientational order and hence broaden the angular scans.

We emphasize here that the angular scan profile obtained from the diffraction geometry represents the true intrinsic orientational order unaffected by any artificial mosaicity due to motion of the samples. To confirm this suggestion, we cooled the films slowly into the crystalline Sm-G phase. If the broadening arose from a mosaic distribution of the domains, one would expect to observe the same broadening in the Sm-G phase. Instead, we observed that the angular scans became sharper and eventually resolution limited, as the samples were cooled deep into the Sm-G phase. This, in turn, means that using this technique we were able to grow very high quality Sm-G single crystals.

We attribute the high degree of hexatic order in these films to the ordering field from the surface layers. A common feature in thin films is enhanced ordering at and near the surface due to the surface tension between the boundary layers and the surrounding gas. Within a quadratic-functional-integral approach, Lyra [24] studied the effect of surface ordering on the profile of the angle fluctuations in hexatic films and defined a characteristic length ξ_K associated with the decay of the surface order into the bulk, where $\ln 2\xi_K \propto \Delta K/K_A$, K_A is the effective Frank constant of each layer, and ΔK is the enhancement of the surface effective Frank constant. In the regime $l \gg \xi_K$, the system becomes more ordered as l increases. However, for $l < \xi_K$, the surface order becomes more relevant—in other words, as the thickness of a sample decreases, the surface ordering field becomes more effective. Hence, one expects that the 60-layer film could show better developed hexatic order than the 200-layer film. This is indeed the case. Specifically, the 60-layer film shows better defined hexatic order than the 200-layer film as represented by the smaller value of the HWHM and the larger values of the harmonic amplitudes (more obvious among higher harmonics) C_{6n}. In both cases the

orientational order is much better defined even well into the hexatic phase than that observed by Noh *et al.* [15] in thick films of TB*n*A and that observed by Brock *et al.* [8] in 8OSI films of various thickness. However, in both the TB5A thick film and 8OSI thin film experiments, the sample was rotated in carrying out the angular scans. This may have introduced an artificial mosaicity in the orientational order. We note that in the 8OSI thin film experiments, efforts were made to reduce the effects of the sample motion by setting the motor drivers at their lowest speeds. No movement of the thin films was observed but nevertheless one cannot rule out absolutely any broadening due to the motion [25].

Previous experiments and theory on thick liquid-crystal films (presumably in the three-dimensional limit) [8,16] have discovered that $C_{6n}=C_6^{\sigma_n}$, where $\sigma_n=n+\lambda n(n-1)$. In mean-field theory where the fluctuations are ignored, the order parameters scale as $C_{6n}\sim C_6^n$, that is, $\lambda\sim 0$. In the two-dimensional limit, where the fluctuations dominate, $C_{6n}\sim C_6^{n^2}$, that is $\sigma_n=n^2$, or, equivalently, $\lambda=1$ [26,27]. We have also fitted the data to Eq. (3) with the form

$$C_{6n}=C_6^{n+\lambda n(n-1)} \tag{4}$$

as predicted by Aharony *et al.* [16]. We find that fits to the angular scans for temperatures right up to the transition temperature yield results identical to those shown by the lines in Fig. 4. The λ values so obtained are plotted in Figs. 7(a) and 7(b) for the 200- and 60-layer films, respectively. The λ values are much different from the theoretical value in the two-dimensional limit ($\lambda=1$ in two dimensions); they also differ from the results obtained by Cheng *et al.* [10] from an electron diffraction study on the smectic-*B* hexatic phase of a four-layer-thick liquid-crystal film of a mixture of 12 wt.% of 4-proprionylphenyl-*trans*-(4-*n*-pentyl)cyclohexane carboxylate (PP5CC) in *n*-hexyl-4′-*n*-pentyloxybiphenyl-4-carboxylate (65OBC). Cheng *et al.* [10] measured C_{6n} for $n=1$, 2, 3, and 4 on a four-layer sample in the untilted hexatic smectic-*B* phase. They obtained an effective $\lambda=0.8$, which was later interpreted as evidence of dimensional crossover [28].

This indicates that although the fluctuations become more and more important as one decreases the sample thickness from the three-dimensional limit to the two-dimensional limit, surface effects apparently increase in relative importance. This is confirmed by the fact that the 60-layer film has an even smaller λ value than the 200-layer film. Presumably, however, there will be another crossover to true two-dimensional ($\lambda=1$) behavior when the films become extremely thin, that is, of order two to four layers [13,14].

IV. CONCLUSION

We conclude that the surface layers provide a strong orientational ordering field that enhances the orientational order in thin TB5A films. Both the 60- and the 200-layer films show very well established hexatic order. We introduce a synchrotron x-ray diffraction geometry, which we have labeled an "*x* scan," to measure the intrinsic line shape of the hexatic phase without any artificial broadening due to the sample motion. In both the 200- and 60-layer films, deep in the hexatic phase, the primary order parameter C_6 is close to 1 and the HWHM of the hexatic line shape is very small.

The transition between the Sm-*C* and the Sm-*F* phases in the TB5A system is strongly first order even in films as thin as 60 layers. The development of the hexatic order parameters was analyzed quantitatively by fitting the data to a Fourier cosine series. The obvious discontinuous jump in all of the order parameters illustrates the strong first order nature of the transition. The character of the transition may also be affected by the presence of the strong ordering field from the surface layers.

Finally, we applied the scaling relation among the harmonics, $C_{6n}\sim C_6^{n+\lambda n(n-1)}$, to describe the growth of the

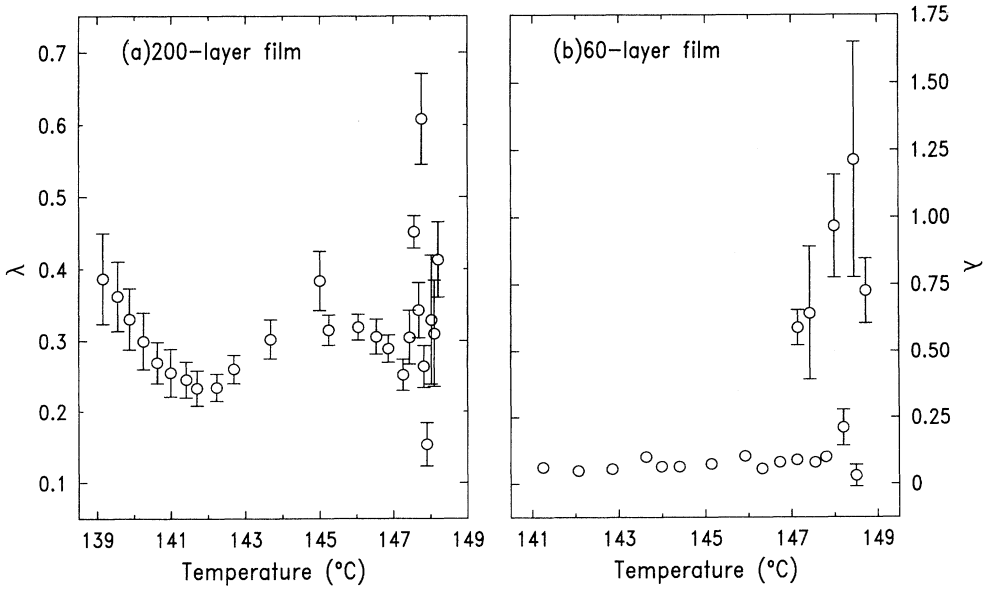

FIG. 7. Temperature dependence of the fitted λ values for both films. Notice that the λ value is not very well determined close to the transition temperature. (a) ~200-layer film. (b) ~60-layer film.

higher order parameters. The resulting values of λ were much smaller than the predicted value of 1 for a two-dimensional system. Indeed, for the 60-layer film λ was close to zero indicating that the system was close to the mean-field regime, consistent with the presence of the surface field that suppresses the thermal fluctuations. Further theoretical and experimental work is required to understand quantitatively the role of the surface layers in the smectic-*F* (Sm-*F*) $\rightarrow$ the smectic-*C* (Sm-*C*) phase transition in thin liquid-crystal films.

ACKNOWLEDGMENTS

We would like to thank J. D. Brock and L. B. Sorensen for helpful discussions of their work. This research was supported by the MRSEC Program of the National Science Foundation under Award No. DMR 94-00334. The work at the National Synchrotron Light Source was supported by the U.S. Department of Energy under Contract No. DE-AC02-76CH00016.

[1] J. M. Kosterlitz and D. J. Thouless, J. Phys. C **6**, 1181 (1973); J. M. Kosterlitz, *ibid.* **7**, 1046 (1974).
[2] B. I. Halperin and D. R. Nelson, Phys. Rev. Lett **41**, 121 (1978).
[3] A. P. Young, Phys. Rev. B **19**, 1855 (1979).
[4] D. R. Nelson and B. I. Halperin, Phys. Rev. B **19**, 2457 (1979).
[5] D. E. Moncton and R. Pindak, Phys. Rev. Lett. **43**, 701 (1979).
[6] R. J. Birgeneau and J. D. Litster, J. Phys. (Paris) **39**, L399 (1978).
[7] J. D. Brock, A. Aharony, R. J. Birgeneau, K. W. Evans-Lutterodt, J. D. Litster, P. M. Horn, G. B. Stephenson, and A. R. Tajbakhsh, Phys. Rev. Lett. **57**, 98 (1986).
[8] J. D. Brock, D. Y. Noh, B. R. McClain, J. D. Litster, R. J. Birgeneau, A. Aharony, P. M. Horn, and J. C. Liang, Z. Phys. B **74**, 197 (1989).
[9] J. D. Brock, R. J. Birgeneau, J. D. Litster, and A. Aharony, Contemp. Phys. **30**, 321 (1989).
[10] M. Cheng, J. T. Ho, S. W. Hui, and R. Pindak, Phys. Rev. Lett. **59**, 1112 (1987); **61**, 550 (1988).
[11] T. Pitchford, G. Nounesis, S. Dumrongrattana, J. M. Viner, C. C. Huang, and J. W. Goodby, Phys. Rev. A **38**, 1938 (1985).
[12] D. Y. Noh, J. D. Brock, J. O. Fossum, J. P. Hill, W. J. Nuttall, J. D. Litster, and R. J. Birgeneau, Phys. Rev. B **43**, 842 (1991).
[13] R. Geer, C. C. Huang, R. Pindak, and J. W. Goodby, Phys. Rev. Lett. **63**, 540 (1989).
[14] R. Geer, T. Stoebe, C. C. Huang, R. Pindak, G. Srajer, J. W. Goodby, M. Cheng, J. T. Ho, and S. W. Hui, Phys. Rev. Lett. **66**, 1322 (1991).
[15] D. Y. Noh, J. D. Brock, J. D. Litster, R. J. Birgeneau, and J. W. Goodby, Phys. Rev. B **40**, 4920 (1989).
[16] A. Aharony, R. J. Birgeneau, J. D. Brock, and J. D. Litster, Phys. Rev. Lett. **57**, 1012 (1986).
[17] J. P. Hill, Ph.D. thesis, Massachusetts Institute of Technology, 1992.
[18] D. R. Nelson and B. I. Halperin, Phys. Rev. B **21**, 5321 (1980).
[19] J. Collett, L. B. Sorensen, and P. S. Pershan, Phys. Rev. A **32**, 1036 (1985).
[20] L. B. Sorensen (private communication).
[21] J. D. Brock, Ph.D. thesis, Massachusetts Institute of Technology, 1987.
[22] R. Pindak, D. E. Moncton, S. C. Davey, and J. W. Woodby, Phys. Rev. Lett. **46**, 1135 (1981).
[23] E. B. Sirota, P. S. Pershan, L. B. Sorensen, and J. Collett, Phys. Rev. A **36**, 2890 (1987); Phys. Rev. Lett. **55**, 2039 (1985); J. Collett, P. S. Pershan, E. B. Sirota, and L. B. Sorensen, *ibid.* **52**, 356 (1984); **52**, 2190(E) (1984).
[24] M. L. Lyra, Phys. Rev. B **47**, 2501 (1992).
[25] J. D. Brock (private communication).
[26] M. Paczuski and M. Kardar, Phys. Rev. Lett. **60**, 861 (1988).
[27] A. Aharony and M. Kardar, Phys. Rev. Lett. **61**, 2855 (1988).
[28] M. Chen, J. T. Ho, S. W. Hui, and R. Pindak, Phys. Rev. Lett. **60**, 862 (1988).